THE SCIMITAR ANTENNA

by

GARY LEE JOHNSON

B. S., Kansas State University, 1961

A MASTER'S THESIS

submitted in partial fulfillment of the

requirements for the degree

MASTER OF SCIENCE

Department of Electrical Engineering

KANSAS STATE UNIVERSITY
Manhattan, Kansas

1963

Approved by:

Harley S. Hoyt
Major Professor

TABLE OF CONTENTS

INTRODUCTION

During the past few years much has been written about spiral antennas, but very little about another broadband antenna known as the scimitar antenna. Experimental and theoretical work relating to this antenna is discussed in this paper. A first-order approximation to the field equations is derived.

In 1941, Schelkunoff, of the Bell Telephone Laboratories, concluded that an antenna of sufficient length, whose shape is defined entirely in terms of angles, should exhibit impedance and radiation characteristics which are independent of frequency. It was not until 1953 that an antenna using this principle was actually developed by Turner, of the Wright-Patterson Air Development Center's Aerial Reconnaissance Laboratory. It had the shape of an Archimedes spiral. The equiangular spiral was developed in 1954 by Rumsey at the University of Illinois, and the log periodic antenna the following year in the same laboratory. The scimitar antenna was developed in 1956 at the Wright-Patterson Air Development Center.

The scimitar antenna, in common with the spiral antennas, is characterized by high efficiency, good mechanical features, no matching networks, and broadband operation over at least a ten-to-one frequency range.

EXPERIMENTAL WORK

Antenna Configuration

Various shapes of scimitar antennas are illustrated in Fig. 1. Spiral antennas are usually composed of two balanced arms each extending over several revolutions. On the other hand, the scimitar antenna extends from zero to 180 degrees only, and it is terminated on a transverse ground plane, as shown in Fig. 2. The angle A shown in Fig. 1a is a constant greater than 90 degrees. This is why the equiangular spiral or scimitar antennas are so named. Equiangular scimitar shape is obtained by using one set of values for a and k on the outer curve, and another set on the inner curve. For a given value of a, commonly used values for k may be .35 for the outer curve and from .25 to .05 for the inner curve, with smaller values yielding less impedance variation with frequency and somewhat higher efficiency of such an antenna.

The equiangular spiral, also known as the logarithmic spiral, has received somewhat more attention than the Archimedes spiral, although both are widely used. The parabolic spiral has not been used to any extent, although it should also operate in the frequency-independent mode as do the other two spirals.

The lower cut-off frequency of both the spiral and scimitar antennas occurs when the maximum diameter of the antenna is approximately one-half wavelength. This fact can be used to determine a scaling factor for the curves given in Fig. 1 when it is

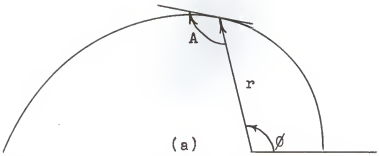

Equiangular or logarithmic spiral. $r = ae^{k\emptyset}$.

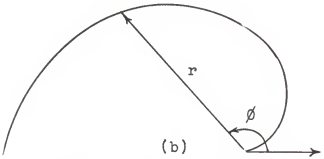

Archimedes spiral. $r = k\emptyset$.

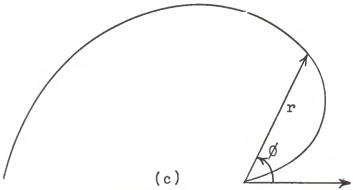

Parabolic spiral. $r^2 = k\emptyset$.

Fig. 1. Empirical shapes of scimitar antennas.

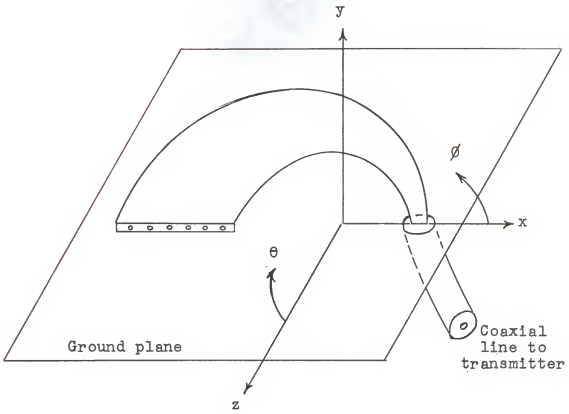

Fig. 2. Equiangular scimitar mounted on ground plane. The large end of the scimitar is electrically connected to the ground plane, whereas the small end is connected by a feed-through insulator to the inner conductor of a 50-ohm coaxial line. The shield of the coaxial line is connected to the ground plane.

desired to construct an antenna which will operate at frequencies down to a known lower cut-off frequency.

There is no definite upper cut-off frequency. The coaxial line feeding the antenna actually is the limiting factor as losses in coaxial line usually become prohibitive above five or six kilomegacycles. Models of the scimitar antenna are known to have been tested at frequencies between 10 and 20 kilomegacycles, with little deterioration in their performance.

Impedance Characteristics

The scimitar antenna has fairly uniform impedance characteristics over a wide range of frequencies. The impedance is known to go through some sharp resonances at certain frequencies below the lower cut-off frequency. Above this lower cut-off frequency, plots of resistance and reactance are relatively flat. Typical plots of resistance and reactance versus frequency are shown in Fig. 3. This data was actually taken for a spiral antenna, (Riblet, 1960), but is believed to be very representative of any scimitar antenna. The characteristic impedance of this antenna is approximately 50 ohms which is essentially resistive at frequencies well above the lower cut-off frequency. The normalized resistance and reactance plotted on a Smith Chart versus frequency resembles a right-handed spiral, moving toward values of lower voltage standing wave ratio, VSWR, as the frequency is increased, as shown in Fig. 4. The Smith Chart has the property that a plot of constant VSWR forms a circle around the origin.

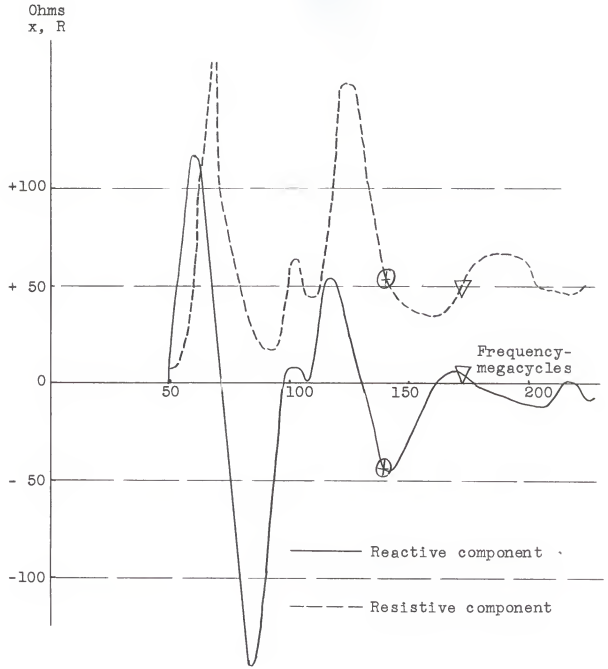

Fig. 3. Typical impedance data for scimitar antenna.

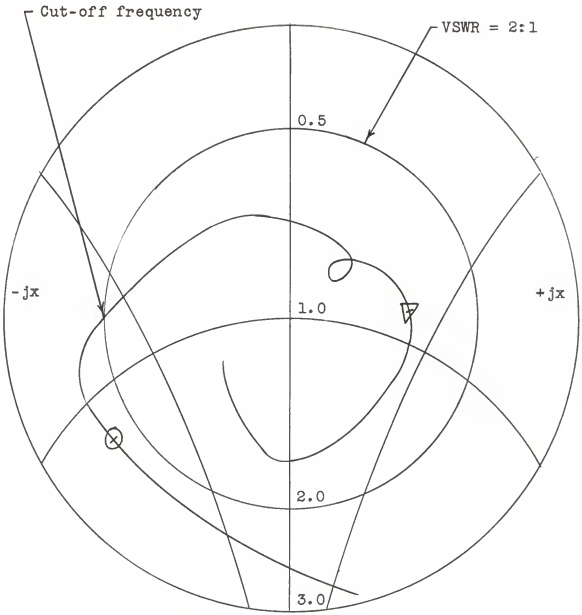

Fig. 4. VSWR versus frequency on a Smith chart.

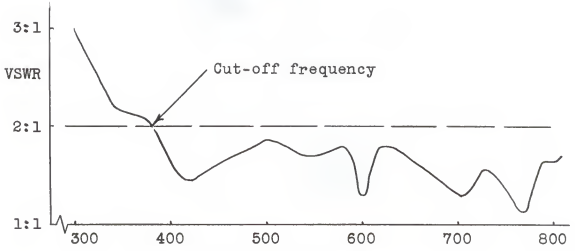

Fig. 5(a). VSWR for equiangular scimitar, $r = ae^{k\phi}$.

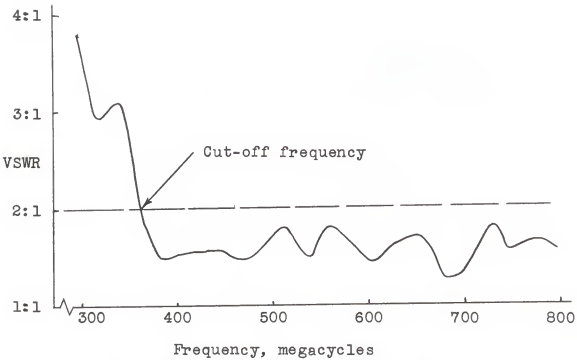

Fig. 5(b). VSWR for Archimedes scimitar, $r = k\phi$.

or two in the plane of the antenna. Some typical radiation patterns are shown in Figs. 6 and 7. The field measurements were made with a dipole antenna held at a constant distance from the origin of the spiral curve. Standard spherical coordinates were used and are shown in Fig. 2.

Polarization of the field is elliptical everywhere except in the plane of the antenna, where it is linear. Some variation in the shape of the field strength pattern is observed as the frequency is varied. This is analogous to the variation noted for spiral antennas where the main lobe is somewhat off center, due to truncation of the arms and the finite-sized feed point. The direction of maximum radiation then changes as the frequency is varied. Although other factors, such as the finite-size and possibly the imperfect conductivity of the ground plane, affect the field pattern of a scimitar antenna, it has the same general variation of the field pattern with frequency as a spiral antenna.

A linearly polarized receiving antenna is usually used as the field is polarized right-handed on one side of the scimitar antenna and left-handed on the other side. A circularly polarized receiving antenna would favor one side of the scimitar, and therefore it would be unsuitable for this purpose. Two linearly polarized antennas oriented at right angles to each other may be required to measure both the horizontal and vertical components under weak signal conditions.

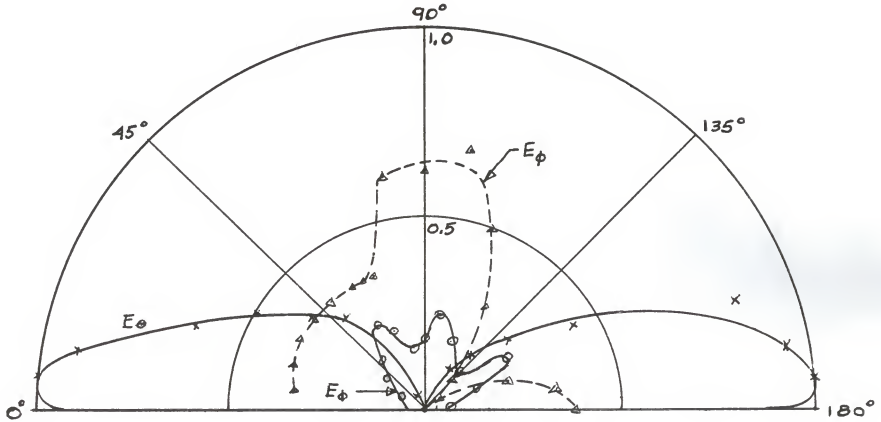

Fig. 6. Experimental field strength patterns for Archimedes scimitar antenna, r = kØ.

Ø = 90°, θ variable.

θ = 90°, Ø variable (E_θ = 0).

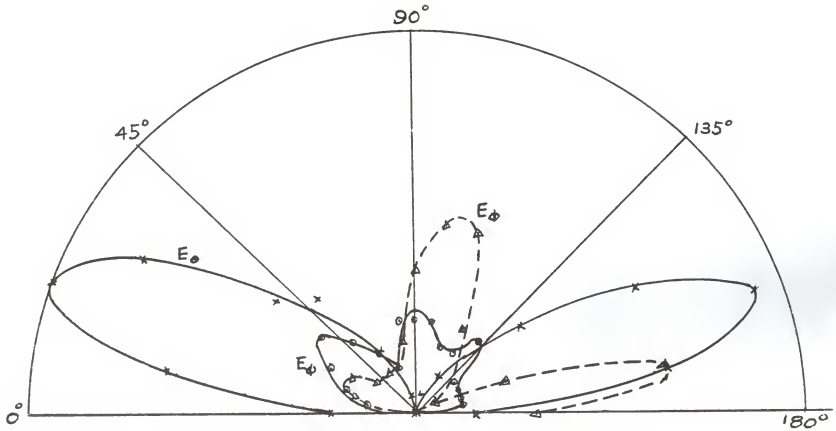

Fig. 7. Experimental field strength patterns for equiangular scimitar antenna, $r = ae^{k\phi}$.

$\phi = 90°$, θ variable.

$\theta = 90°$, ϕ variable ($E_\theta = 0$).

THEORETICAL CALCULATIONS

Equations of Model Antennas

It is desirable, for comparison of experimental results, to construct the equiangular scimitar as similar to the Archimedes scimitar as possible, even though the antennas are defined by different equations. For this purpose as well as for the solution of some theoretical problems, arc lengths of the spiral curves must be derived, using standard methods of the calculus.

The equation of the equiangular spiral is $r = ae^{k\phi}$, and it may be expressed in cartesian components as:

$$x = r \cos \phi = ae^{k\phi} \cos \phi$$

$$y = r \sin \phi = ae^{k\phi} \sin \phi$$

$$\frac{dx}{d\phi} = - ae^{k\phi} \sin \phi + ake^{k\phi} \cos \phi$$

$$\frac{dy}{d\phi} = ae^{k\phi} \cos \phi + ake^{k\phi} \sin \phi$$

The incremental arc length is then

$$\left[\left(\frac{dx}{d\phi}\right)^2 + \left(\frac{dy}{d\phi}\right)^2\right]^{\frac{1}{2}} = ae^{k\phi} \sqrt{k^2 + 1}$$

The distance along the spiral from $\phi = 0$ to an arbitrary ϕ is

$$b_e = \int_0^{\phi} ae^{k\phi} \sqrt{k^2 + 1} \; d\phi = \frac{a\sqrt{k^2 + 1}}{k} \left[e^{d\phi} - 1\right] \qquad (1)$$

The length of the equiangular spiral for one-half revolution is

$$L_e = \frac{a\sqrt{k^2 + 1}}{k}\left[e^{k\pi} - 1\right] \tag{2}$$

Similar results for the Archimedes spiral, $r = k\phi$, are calculated as:

$$b_a = \int_0^{\phi} k\sqrt{\phi^2 + 1}\, d\phi = k\left\{\tfrac{1}{2}\left[\phi\sqrt{\phi^2 + 1} + \ell n\,(\phi + \sqrt{\phi^2 + 1})\right]\right\} \tag{3}$$

$$L_a = 6.09\ k \tag{4}$$

This elementary calculus technique fails to yield proper results for the parabolic spiral because of a first-order pole in the integrand at $\phi = 0$. More advanced techniques can be used but since the parabolic scimitar has found little or no application to date, it will not be discussed further.

Two criteria were established for comparing experimental results of the two types of scimitar antennas. These are:

(a) $r_e = r_a$ at $\phi = \pi$

(b) $L_e = L_a$

(a) $ae^{k_e\pi} = k_a\pi$

Consider $k_a = 1$. Then

$$L_a = 6.09\ k_a = 6.09$$

and

$$L_e = L_a = 6.09 = \frac{a\sqrt{k_e^2 + 1}}{k_e}\left[e^{k_e\pi} - 1\right]$$

A solution of these equations gives

$$k_e = .39,\ a = .90$$

The subscript e refers to equiangular, and a to Archimedes. The subscripts may not be used if it is clear from the context which antenna is being discussed.

Both a and k_a will be multiplied by a common scaling factor in order to construct antennas of different sizes, and this will not change their relative characteristics used in their comparison.

Methods of Solution of Field Equations

A classical method of deriving the field of an antenna is to assume or obtain a current distribution, integrate this current distribution to find $\bar{A}$, the vector magnetic potential, and take the curl of curl of $\bar{A}$ to obtain the electric field intensity $\bar{E}$ (Hayt, 1958, Stratton, 1941).

The vector potential can be expressed as

$$\bar{A}(u, t) = \frac{\mu}{4\pi} \oint \frac{1}{R_1} \bar{I}(u', t^*) dL \qquad (5)$$

where the vector property of the integrand has arbitrarily been associated with the current rather than the conductor in which it flows. The symbol u represents the coordinate triplet (x, y, z) of the point in space where the vector potential is desired, and u' represents (x', y', z') of a point on the antenna where the current element dL is located. The retarded time is expressed as $t^* = t - \frac{R_1}{U}$, where U is the velocity of propagation and R_1 is the distance from the current element dL to the point (x, y, z). These quantities are illustrated in Fig. 8 for a general current element. Expressions for R_1, $\bar{I}$, and dL for the particular case of a scimitar antenna are obtained in this section.

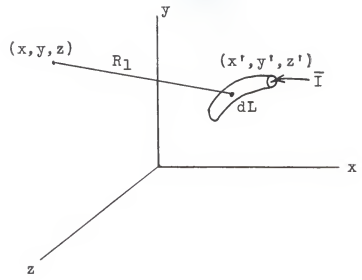

Fig. 8. The vector potential at (x, y, z) due to a current $\bar{I}$ in dL at (x', y', z').

The difficult part of this approach is the integration of Eq. (5). Other means of solution have been attempted in order to get around this difficulty. Some of the approximate solutions have been applied to spiral antennas of several revolutions and are discussed here briefly to indicate why these cannot be applied to an analysis of scimitar antennas.

Curtis (1960) approximated the spiral antenna with a series of semicircular arcs and used symmetry about an axis through the origin to determine the far field. This is a good approximation for a tightly wound spiral only. It is not valid in the case of a scimitar for various reasons. The scimitar is not symmetric about any axis or point. This method does not allow for the ground plane which is essential to the scimitar's operation. Also the scimitar cannot be approximated by a semicircle as well

as a tightly wound spiral because of different constants in the defining equations.

Rumsey (1961 a, b) solved Maxwell's equations for the case of circularly polarized surface waves propagating along anisotropic sheets which are perfectly conducting in one tangential direction and perfectly transparent in the orthogonal tangential direction. The two-arm spiral is approximated by a sheet containing an infinite number of spirals extending out a large distance. The problem was solved under this approximation and the results were found to agree closely with those obtained experimentally using finite antennas. It seems that the rapid decrease in antenna current, as the distance from the input is increased, causes the truncated antenna to have essentially the same characteristics as the infinite structure.

Again, this method is not valid in the case of the scimitar antenna because it does not consider the ground plane; it uses symmetry conditions not present in the scimitar antenna, and it does not allow for a finite (nonzero) current at the junction of the antenna and its ground plane.

The Current Distribution

The calculation of the vector magnetic potential involves the integration of the current distribution of the antenna. The current distribution in the scimitar antenna is assumed to be somewhat similar to that measured in spiral antennas. Dyson (1957) has measured the current and phase distribution of several

equiangular spirals at different frequencies. The validity of this assumption cannot be justified without actual measurement, a rather difficult task, but experimental results seem to indicate this to be a reasonably satisfactory assumption.

Typical amplitude and phase variation along one arm of a balanced equiangular spiral are shown in Fig. 9. The phase varies almost linearly with distance measured along the antenna arm from the feed point for about the first two wavelengths. In the first wavelength from the feed point, the phase has changed about 360 degrees, which is reasonable.

The current amplitude decreases along the antenna arm as a result of ohmic losses and radiation. The current in this particular case is about 15 decibels below the input level at one wavelength from the feed point. This figure varies between eight and 18 decibels down for various equiangular spirals in the frequency range of, say, 500 to 5000 megacycles.

The operating efficiency of the scimitar antenna increases from near zero to above 60 per cent as the length of its outer curve approaches one wavelength long or more as the frequency is increased. The assumption follows that the scimitar has a current amplitude and phase distribution similar to that of the first wavelength of the equiangular spiral antenna arm, as shown in Fig. 10. The distribution is essentially a current sheet with a somewhat higher current density toward the outside of the curve. Lines of constant phase are approximately orthogonal to the spiral curves.

It might appear that the current would flow parallel to one

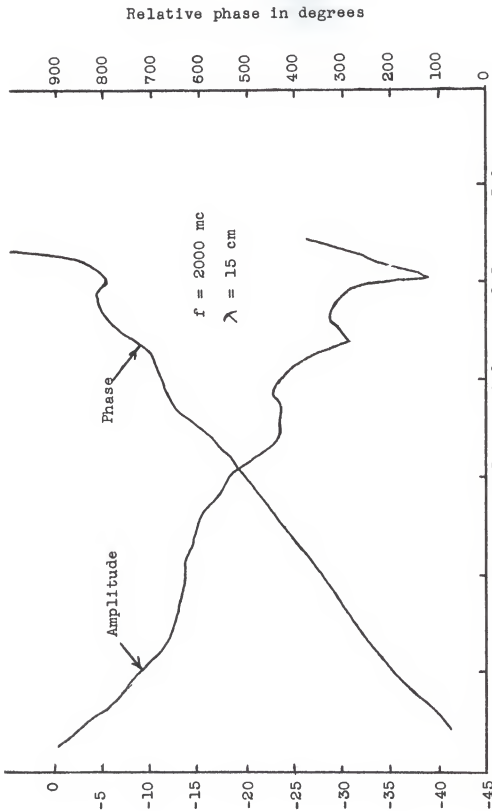

Fig. 9. Relative amplitude and phase of current along arm of balanced equiangular spiral, k = .30, a = .75. Length of antenna arm = 40 cm.

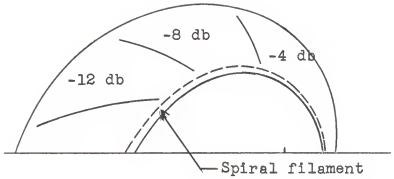

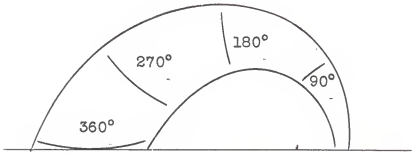

Fig. 10. Assumed contours of equal phase and amplitude of current distribution in equiangular scimitar antenna.

of the spiral filaments making up the antenna (Fig. 10). The direction of current flow as measured by Dyson indicates otherwise. The direction of current 1.5 wavelengths from the feed point showed a variation of up to 10 or 15 degrees from the expected direction along the filaments. The direction of current flow varied from the expected direction by as much as 55 degrees at greater distances from the feed point. The variation does not seem to be expressible mathematically. Since the scimitar antenna begins to operate efficiently with an antenna arm length of less than 1.5 wavelengths, not much error will be introduced by assuming that the antenna current flows parallel to the spiral filaments forming the antenna.

An Expression for the Vector Magnetic Potential $\overline{A}$

The vector potential will be derived for the case of a thin scimitar antenna of sufficiently small width that the width need not be considered in the calculations. It will be further shown that the theoretical field calculated for a narrow antenna agrees for the most part with the experimental field of actual antennas of the relative dimensions shown in Fig. 10.

Cylindrical and spherical coordinates are used interchangeably in finding the expression for $\overline{A}$. The various quantities appearing in $\overline{A}$ are illustrated in Fig. 11. The distances r and R_0 lie always in the z = 0 plane, while R_1 may have a component in the z direction. The letter R is reserved for the radius of spherical coordinates. The point at which $\overline{A}$ is desired is

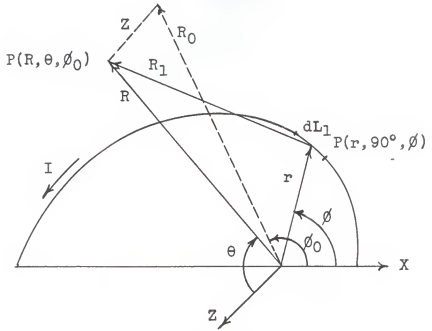

Fig. 11. A thin equiangular scimitar antenna.

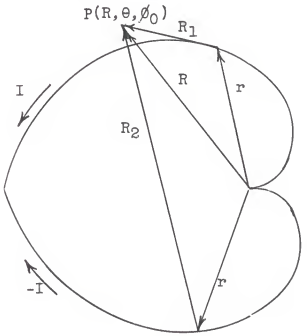

Fig. 12. A thin Archimedes scimitar antenna with image antenna.

designated as $P(R, \theta, \phi_0)$, while the location of the current element is $P(r, 90°, \phi)$. These correspond to the coordinate triplets u' and u, respectively, which were mentioned earlier. The symbols used in the two coordinate systems are nonambiguous with the possible exception of the unit vector $\bar{a}_r$ which will be handled by letting $\bar{a}_{rc}$ be the $\bar{a}_r$ vector in cylindrical coordinates and $\bar{a}_{rs}$ in spherical coordinates. They are related by this expression:

$$\bar{a}_{rc} = \bar{a}_{rs} \sin\theta + \bar{a}_\theta \cos\theta \tag{8}$$

The distance R_1 from the current element dL_1 is evaluated in terms of r and R_0 to simplify the integration. In terms of cylindrical coordinates,

$$R_1^2 = R_0^2 + r^2 - 2rR_0 \cos(\phi - \phi_0) + z^2$$

Then in spherical coordinates, substituting R sin θ for R_0, and R cos θ for z,

$$R_1 = \sqrt{(R \sin\theta)^2 + r^2 - 2r(R \sin\theta)\cos(\phi - \phi_0) + (R\cos\theta)^2}$$

$$= R\sqrt{1 + \frac{r^2}{R^2} - \frac{2r}{R}\sin\theta\cos(\phi - \phi_0)} \tag{9}$$

The retarded current can be expressed as

$$\bar{I}(u', t^*) = \bar{I}_0 e^{j\left[\omega(t - R_1/U) - b\right]} \tag{10}$$

where $I_0 e^{j\omega t}$ is the form of the current at the antenna input and $I_0 e^{j(\omega t - b)}$ is the current at a point on the antenna. The letter b may be a complex quantity in order to allow for both phase shift and amplitude attenuation as the current wave moves along the antenna. The $e^{-j(R_1\omega/U)}$ term takes into account the phase difference between a point on the antenna, $P(r, 90°, \phi)$, and a

point in space, P(R, θ, ϕ_0), in a medium with velocity of propagation U.

The direction of the current element for the equiangular scimitar may be expressed as

$$d\bar{L}_1 = rd\phi\ \bar{a}_\phi + dr\bar{a}_{rc} = ae^{k\phi}\ d\phi\ \bar{a}_\phi + ake^{k\phi}\ d\phi\ \bar{a}_{rc}$$

$$= ae^{k\phi}\ d\phi\ \bar{a}_\phi + ake^{k\phi}\ d\phi(\bar{a}_{rs} \sin\theta + \bar{a}_\theta \cos\theta)$$

and for the Archimedes scimitar as

$$d\bar{L}_1 = k\phi d\phi\ \bar{a}_\phi + kd\phi(\bar{a}_{rs} \sin\theta + \bar{a}_\theta \cos\theta) \qquad (11)$$

The variable part of the quantity b (omitting complex constant multipliers) is given by Eq. (1) for the equiangular scimitar, and by Eq. (3) for the Archimedes scimitar.

The ground plane and the current flowing in it must also be considered in the expression for the field. Kraus (1950) suggests that an antenna and its ground plane may be replaced by the antenna and its image for the purpose of determining the field. An equal and opposite current flows in the image antenna as compared with the real antenna, as shown in Fig. 12. The assumption is made that the ends of the real and image antennas do not touch each other because image theory cannot be applied otherwise.

It is evident that the angle between r, the radius of the image antenna, and R_0 is $\phi + \phi_0$. This yields for R_2

$$R_2 = R\sqrt{1 + \frac{r^2}{R^2} - \frac{2r}{R} \sin\theta \cos(\phi + \phi_0)}$$

The expression for the vector magnetic potential may now be written.

$$\bar{A}(u, t) = \int \frac{\mu \bar{I}_1(u', t^*)}{4\pi R_1}\ dL_1$$

$$= \frac{\mu}{4\pi} \int_{\phi=0}^{\pi} \frac{I_0 e^{j\left(\omega t - b - (R_1\omega/U)\right)}}{R_1} \left(r d\phi\, \bar{a}_\phi + dr \bar{a}_{rc}\right)$$

$$+ \frac{\mu}{4\pi} \int_{\phi=0}^{-\pi} \frac{(-I_0) e^{j\left(\omega t - b - (R_2\omega/U)\right)}}{R_2} \left(r d\phi(-\bar{a}_\phi) + dr\, \bar{a}_{rc}\right) \qquad (12)$$

This expression for $\bar{A}$ is valid for both the equiangular and the Archimedes scimitar as long as the appropriate expressions for b and r are used. Since the two integrals are very similar, the same approximations and techniques of integration should apply to both, and therefore only the first integral of Eq. (12), as applied to the Archimedes scimitar, is solved for a general theoretical expression containing b and $k\phi$. The integral under consideration becomes

$$\bar{A} = \int_{\phi=0}^{\pi} \frac{\mu I_0\, e^{j\left(\omega t - c_1 b_a - (R_1\omega/U)\right)}}{4\pi R_1} \left(k\phi d\phi\, \bar{a}_\phi + k d\phi\, \bar{a}_{rc}\right) \qquad (13)$$

where b_a and R_1 are given by Eqs. (3) and (9), respectively.

This expression for $\bar{A}$ has been obtained using the following assumptions.

1. The velocity of propagation along the antenna is constant for a particular frequency.
2. The electrical length of the antenna is one full wavelength or perhaps an integral multiple of a wavelength. This information is included in c_1 as well as any attenuation factors due to ohmic losses or radiation.
3. This expression is derived for a narrow Archimedes scimitar antenna, although it will be shown that the results agree for the most part with those obtained

experimentally for "wide" antennas.

4. Image theory is valid for this particular case.

APPROXIMATE FIELD EXPRESSION

Approximation to the Vector Magnetic Potential Integral Equation

The vector potential has been expressed as

$$\bar{A}(u,t) = \frac{\mu}{4\pi} \int \frac{1}{R_1} \bar{I}(u', t^*)dL \tag{5}$$

Since $\bar{I}(u', t^*)$ is bounded, and in fact a monotonically decreasing function of distance along the antenna, $\bar{A}$ is a continuous function of the coordinates (u), i.e., (R, θ, ϕ_0), possessing continuous first and second derivatives at every point. In other words, the integrand is uniformly continuous and operations of differentiation and integration may be interchanged, at least with respect to the coordinates (u). An expression for $\bar{E}$ can now be obtained prior to the integration of Eq. (5). Thus for free space

$$\bar{B} = \nabla \times \bar{A}(u,t) = \frac{\mu}{4\pi} \int \nabla \times \left(\frac{\bar{I}(u', t^*)}{R_1} \right) dL \tag{14}$$

where ∇ is the vector operator and is a function of the coordinates R, θ, and ϕ_0. The integrand of Eq. (14) can be expanded by using the vector identity $\nabla \times c\bar{C} = c\nabla \times \bar{C} + \nabla c \times \bar{C}$ into the form

$$\bar{B} = \frac{\mu}{4\pi}\int\left(\frac{1}{R_1}\nabla \times \bar{I} + \nabla\left(\frac{1}{R_1}\right) \times \bar{I}\right) dL \qquad (15)$$

Then for an $e^{j\omega t}$ time variation, and using one of Maxwell's equations,

$$\bar{E} = \frac{1}{j\omega\epsilon\mu}\nabla \times \bar{B} = \frac{1}{j4\pi\omega\epsilon}\int\left[\nabla \times \left(\frac{1}{R_1}\nabla \times \bar{I} + \nabla\left(\frac{1}{R_1}\right) \times \bar{I}\right)\right] dL$$

$$= \frac{1}{j4\pi\omega\epsilon}\int\left[\frac{1}{R_1}\nabla \times (\nabla \times \bar{I}) + \nabla\frac{1}{R_1} \times \nabla \times \bar{I} + \bar{I} \cdot \nabla(\nabla\frac{1}{R_1}) - \nabla\frac{1}{R_1} \cdot \nabla\bar{I} + \nabla\frac{1}{R_1}(\nabla \cdot \bar{I}) - \bar{I}(\nabla \cdot \nabla\frac{1}{R_1})\right] dL \qquad (16)$$

The vector potential $\bar{A}$ is defined such that $\nabla \cdot \bar{A} = 0$, and therefore

$$\nabla \cdot \bar{A} = \frac{\mu}{4\pi}\int\nabla \cdot \frac{\bar{I}}{R_1} dL = \frac{\mu}{4\pi}\int\left[\frac{1}{R_1}\nabla \cdot \bar{I} + \bar{I} \cdot \nabla\frac{1}{R_1}\right] dL \qquad (17)$$

$$= 0$$

The gradient of zero is still zero, so

$$\frac{1}{j\omega\epsilon\mu}\nabla(\nabla \cdot \bar{A}) = \frac{1}{j4\pi\epsilon\omega}\int\left[\nabla(\frac{1}{R_1}\nabla \cdot \bar{I}) + \nabla(\bar{I} \cdot \nabla\frac{1}{R_1})\right] dL$$

$$= \frac{1}{j4\pi\omega\epsilon}\int\left[\frac{1}{R_1}\nabla(\nabla \cdot \bar{I}) + (\nabla \cdot \bar{I})\nabla\frac{1}{R_1} + \bar{I} \cdot \nabla(\nabla\frac{1}{R_1}) + \nabla\frac{1}{R_1} \cdot \nabla\bar{I} + \bar{I} \times (\nabla \times \nabla\frac{1}{R_1}) + \nabla\frac{1}{R_1} \times (\nabla \times \bar{I})\right] dL = 0 \qquad (18)$$

The terms of $\bar{E}$ and $\nabla(\nabla \cdot \bar{A})$ may be compared and it is observed that $\bar{E}$ contains all the terms of $\nabla(\nabla \cdot \bar{A})$ plus a term involving ∇^2, the vector Laplacian. Thus the terms which add to zero may be dropped, resulting in

$$\bar{E} = \frac{1}{j\omega \epsilon 4\pi} \int \left(-\frac{1}{R_1} \right) \nabla \bar{I} \, dL$$

$$= \frac{1}{j4\pi\omega\epsilon} \int \left[\frac{1}{R_1} \nabla \times \nabla \times \bar{I} - \frac{1}{R_1} \nabla (\nabla \cdot \bar{I}) \right] dL \qquad (19)$$

This expression is valid for any realizable current distribution. Certain simple assumptions have been made about $\bar{I}$ and $\bar{A}$, and listed at the close of the preceding section, in order to simplify the solution in the case of a scimitar antenna. The information available at this time indicates that these assumptions do not seem to substantially affect the accuracy of Eqs. (10) or (19).

It is informative to evaluate Eq. (19) in terms of more explicit functions with the aid of several approximations. This permits the electric field intensity in the far field to be plotted directly from the explicit functions. A first-order approximation of the far field, which is the primary area of interest, can be calculated without using a computer. A more accurate treatment of both the near and far fields would definitely make it necessary to use a computer.

First we examine b, which appears in the exponent of Eq. (10). A good approximation for b is a second-order polynomial in ϕ. The use of numerical methods of curve fitting gives

$$b_a = \frac{k}{2} \left[\phi \sqrt{\phi^2 + 1} + \ell n(\phi + \sqrt{\phi^2 + 1}) \right]$$

$$\cong k \left[.35 \, \phi^2 + .83 \, \phi \right] \qquad 0 \leqslant \phi \leqslant \pi \qquad (20)$$

and

$$b_e = \frac{a\sqrt{k^2+1}}{k}\left[e^{k\phi} - 1\right] \cong a(1.072)\left[.154\ \phi^2 + .3\ \phi\right] \qquad 0 \leq \phi \leq \pi \tag{21}$$

for the particular case of k = .39.

The distance

$$R_1 = R\sqrt{1 + \frac{r^2}{R^2} - \frac{2r}{R}\sin\theta\cos(\phi - \phi_0)} \tag{9}$$

can be simplified by neglecting the quantity r^2/R^2 when $R >> r$. Neglecting higher order terms and using the binomial theorem, Eq. (9) becomes

$$R_1 = R\left[1 - \frac{2r}{R}\sin\theta\cos(\phi - \phi_0)\right]^{1/2} \cong R\left[1 - \frac{r}{R}\sin\theta\cos(\phi - \phi_0)\right] \tag{22}$$

and

$$\frac{1}{R_1} = \frac{1}{R}\left[\frac{1}{1 - r/R\ \sin\theta\cos(\phi - \phi_0)}\right] \cong \frac{1}{R}\left[1 + \frac{r}{R}\sin\theta\cos(\phi - \phi_0)\right] \tag{23}$$

These are valid approximations for sufficiently large R, but another expression valid for small R, or points close to the antenna, is also needed. The smallest value of R which is permitted for all θ and ϕ_0 is $R = r_{max} + \epsilon$, where ϵ is a small positive number. In other words, a measuring probe is not allowed to touch the antenna as $\bar{A}$ is not defined on conducting surfaces. A closer examination of Eqs. (22) and (23) indicates that these approximations are fair approximations even for R of the same order of magnitude as r. Plots of actual values of

$1/R_1$, from Eq. (9), and the approximate values of Eq. (23) for ϕ_0 equal to 0 degrees, 90 degrees, and 180 degrees, and θ equal to 90 degrees, are given in Fig. 13. The following normalized values of R, r, and k were used for the Archimedes scimitar: $R = r_{max} = k\phi_{max} = k\pi = 1$; $k = 1/\pi$.

It may be seen from Fig. 13 that when ϕ_0 is 0 degrees or 180 degrees, the actual and approximate values of $1/R_1$ agree such that the approximate value is useful, but such is not the case for ϕ_0 in the middle of its range about 90 degrees. A weighted approximation was tried for $1/R_1$, and it resulted in a better fit for ϕ_0 in the middle of its range without affecting the fit of the curves for ϕ_0 equal to either zero degrees or 180 degrees. This weighted approximation was found to be

$$\frac{1}{R_1} \cong \frac{1}{R}\left[1 + \frac{r}{R}\left(\cos(\phi - \phi_0) + \sin(\phi + 30^\circ)\sin\phi_0\right)\sin\theta\right] \tag{24}$$

Equation (24) is therefore used in place of Eq. (23) for the $1/R_1$ multiplying Eq. (19).

The retarded current $\bar{I}(u', t^*)$ in Eq. (19) has been expressed as

$$\bar{I}(u', t^*) = \bar{I}_0\, e^{j\left[\omega(t - R_1/U) - b\right]} \tag{10}$$

where R_1 appears in the exponent and is expressed there in analogy with Eqs. (24) and (22), as

$$R_1 \cong R\left[1 - \frac{r}{R}\sin\theta\left(\cos(\phi - \phi_0) + \sin(\phi + 30^\circ)\sin\phi_0\right)\right] \tag{25}$$

The vector nature of $\bar{I}$ may be expressed in a more explicit fashion as

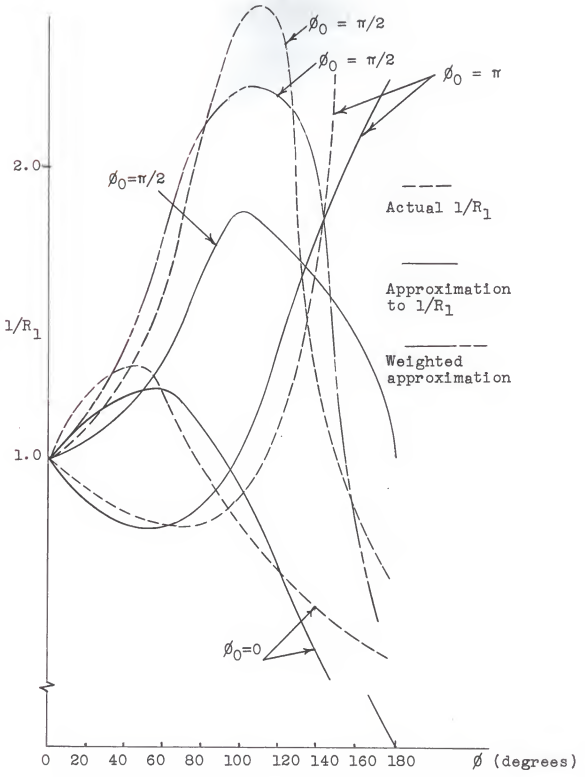

Fig. 13. Comparison of actual, Eq. 9, and approximate values of $1/R_1$, Eq. 23.

$$\bar{I} = I_0 \, e^{j\left[\omega(t-R_1/U)-b\right]} \; k\left[\emptyset \; \bar{a}_\emptyset + \sin\theta \bar{a}_{rs} + \cos\theta \bar{a}_\theta\right]$$

$$= C_2 \, e^{-j\,\omega/U\,R_1} \; k\left[\emptyset \; \bar{a}_\emptyset + \sin\theta \bar{a}_{rs} + \cos\theta \bar{a}_\theta\right] \qquad (26)$$

Here R_1 is the only term in the exponent which is a function of the variables R, θ, and $\emptyset_0$, and hence the other terms can be lumped into C_2 for the purpose of evaluating the vector Laplacian of $\bar{I}$. This evaluation is straightforward but lengthy, and therefore only the result is given. The component of $\nabla \times \nabla \times \bar{I}$ in the $\bar{a}_\theta$ direction is

$$\left[\nabla \times \nabla \times \bar{I}\right]_\theta = C_2 \, e^{-j\,\omega/U\,R_1} \left[\frac{\cos\theta}{R^2 \sin\theta} \left(j\frac{\omega}{U} k\emptyset\right)\left(\emptyset\left[\sin(\emptyset - \emptyset_0) + \cos\emptyset_0 \sin(\emptyset + 30°)\right] + \cos(\emptyset - \emptyset_0) - \sin\emptyset_0 \sin(\emptyset + 30°)\right) \right.$$

$$+ \frac{\cos\theta}{R^2} \left\{ \emptyset\left(j\frac{\omega}{U} k\emptyset\right)\left(\cos(\emptyset - \emptyset_0) + \sin\emptyset_0 \sin(\emptyset + 30°)\right) \right.$$

$$\left. - j\frac{\omega}{U} k\emptyset \left(\sin(\emptyset - \emptyset_0) + \cos\emptyset_0 \sin(\emptyset + 30°) + \frac{\emptyset}{\sin\theta}\right)\right\}$$

$$\cdot \left(j\frac{\omega}{U} k\emptyset\right)\left(\sin(\emptyset - \emptyset_0) + \cos\emptyset_0 \sin(\emptyset + 30°)\right)$$

$$\left. + j\frac{\omega}{U} \frac{\cos\theta}{R} + \frac{\omega^2}{U^2} \cos\theta - j\frac{\omega}{U}\left(j\frac{\omega}{U} k\emptyset\right) \frac{\sin 2\theta}{2R} \left(\cos(\emptyset - \emptyset_0) + \sin\emptyset_0 \sin(\emptyset + 30°)\right)\right] \qquad (27)$$

Similar expressions follow for the other components in which these substitutions are used.

$$a_1 = j\frac{\omega}{U} \qquad a_2 = j\frac{\omega k\emptyset}{U}$$

$$a_3 = \cos(\emptyset - \emptyset_0) + \sin(\emptyset + 30°) \sin\emptyset_0$$

$$a_4 = \sin(\phi + 30^\circ)$$

$$\left[\nabla x \nabla x \bar{I}\right]_\phi = C_2 e^{-j\omega/U R_1} \left[\frac{\phi a_1}{R} - \frac{a_1}{R} \sin\theta\left(\sin(\phi - \phi_0) + a_4 \cos\phi_0\right) - a_1^2\phi + \frac{a_1\phi}{R} + \frac{\phi}{R^2} \frac{\cos^2\theta}{\sin^2\theta} + \frac{\phi a_2 a_3}{R^2} \sin\theta - \frac{a_2}{R^2} \sin\theta\left(\sin(\phi - \phi_0) + a_4 \cos\phi_0\right) + \frac{\phi}{R^2} - \frac{\cos^2\theta (a_2 a_3)^2}{R^2} \phi + \frac{a_2^2 a_3}{R^2} \cos^2\theta\left(\sin(\phi - \phi_0) + a_4 \cos\phi_0\right) - \frac{\phi a_2 a_3 \cos^2\theta}{R^2 \sin\theta}\right] \quad (28)$$

$$\nabla(\nabla \cdot \bar{I})_\theta = C_2 \frac{e^{-j\omega/U R_1}}{R} \left[- a_1 \cos\theta + \frac{2\cos\theta}{R} + \frac{-2\sin\theta \sin 2\theta - \cos 2\theta \cos\theta}{R \sin^2\theta} - \frac{a_2 a_3}{R} 2\cos\theta \sin\theta - a_1 \sin\theta + \frac{2\sin\theta}{R} + \frac{\cos 2\theta}{R \sin\theta} + \frac{a_2 a_3 \cos^2\theta}{R} + \frac{\phi a_2}{R}\left(\sin(\phi - \phi_0) + a_4 \cos\phi_0\right)\right] \quad (29)$$

$$\nabla(\nabla \cdot \bar{I})_\phi = \frac{C_2 e^{-j\omega/U R_1}}{R \sin\theta} \left[\frac{a_2 \cos^2\theta}{R}\left(\sin(\phi - \phi_0) + a_4 \cos\phi_0\right) - \frac{\phi a_2}{R}\left(\cos(\phi - \phi_0) + a_4 \sin\phi_0\right) + \left(a_2 \sin\theta\left[\sin(\phi - \phi_0) + a_4 \cos\phi_0\right]\right) \cdot \left(- a_1 \sin\theta + \frac{2\sin\theta}{R} + \frac{\cos 2\theta}{R \sin\theta} + \frac{a_2 a_3 \cos^2\theta}{R} + \frac{\phi a_2}{R}\left[\sin(\phi - \phi_0) + a_4 \cos\phi\right]\right)\right] \quad (30)$$

The component in the R direction is not considered as there is no

electric field component in this direction in the far field.

Components of Eq. (19) may now be expressed as

$$E_1 = \frac{1}{j4\pi\omega\epsilon} \int_0^{\pi} kC_2 \, e^{-j\,\omega/U\, R_1} \left[\frac{f_1}{R} + \frac{f_2}{R^2} + \frac{f_3}{R^3} + \frac{f_4}{R^4} \right] d\phi \qquad (31)$$

where the f_i represent functions of θ, ϕ, and ϕ_0 obtained from the preceding equations. All terms except f_1/R are assumed negligible in the calculation of the far field. This effects considerable simplification so that the E_1 may now be expressed as follows.

$$E_\theta = \frac{I_0 k}{j4\pi\omega\epsilon} \frac{\omega^2}{U^2} \int_0^{\pi} \frac{\cos\theta}{R} e^{j\omega\left[t - b/\omega - R_1/U\right]} d\phi$$

$$= \frac{I_0 k\omega}{j4\pi\epsilon U^2} e^{j\omega t} \int_0^{\pi} \frac{\cos\theta}{R} e^{-j(b+R_1/U)} \, d\phi \qquad (32)$$

The quantity b given as Eqs. (1) and (3) and appearing in Eq. (32) is a function of ϕ only for a given antenna and may be approximated by a polynomial in ϕ as

$$b = b_1\phi^2 + b_2\phi$$

If R_1 is replaced by Eq. (25) and the first term factored out of the integral, the following expression for the electric field results.

$$E_\theta = C_3 \int_0^{\pi} \cos\theta \, e^{-jk\left[b_1\phi^2 + b_2\phi - \phi \frac{\omega}{U} \sin\theta\left(\cos(\phi - \phi_0) + \sin(\phi + 30^\circ) \sin\phi_0\right)\right]} d\phi \qquad (33)$$

$$C_3 = \frac{I_0 k\omega \, e^{j\omega(t - R/U)}}{j4\pi\epsilon U^2 R}$$

Similarly, the $\bar{a}_\phi$ component is calculated to be

$$E\phi = C_3 \int_0^{\pi} \phi \, e^{-jk\left[f(\phi)\right]} \, d\phi \qquad (34)$$

where the $f(\phi)$ in the brackets is the same as the bracketed expression in Eq. (33).

Equations (33) and (34) are now in an approximated form representing the far field of the Archimedes scimitar. The use of a computer is necessary in order to obtain the complete field patterns as well as to investigate all the possible variations of parameters. However, Eqs. (33) and (34) are integrable directly for certain special cases. This permits a check on their validity by comparison with experimental results, and from it one can infer the general shape of the field patterns. The computer program for this integration, if used, needs to be very versatile. There are several parameters which vary more or less independently of each other. Values of k_a, k_e, and a vary for different antennas. The velocity of propagation along the antenna is not known exactly and may possibly be a function of frequency. Variation in ω over at least a ten-to-one range would have to be considered in the program. The attenuation of the current along the antenna varies between antennas and its effect would also have to be considered. Variation of all these parameters would yield a large amount of data which could take several months for a complete analysis.

Integration to Determine the Electric Field Intensity

The electric field is obtained by integration of Eqs. (33) and (34), and this integration is outlined in this section.

The exponent in brackets of Eq. (33) becomes in the special case of $\phi_0 = 90°$, for example

$$f(\phi) = b_1\phi^2 + b_2\phi - \frac{\omega}{U}\phi \sin\theta\left(\cos(\phi - \phi_0) + \sin(\phi + 30°) \sin\phi_0\right)$$

$$= b_1\phi^2 + b_2\phi - \frac{\omega}{U}\phi \sin\theta\left(\tfrac{1}{2}\cos\phi + 1.866 \sin\phi\right)) \qquad (35)$$

If the variation of ϕ over the range of zero to 180 degrees is divided into two or three ranges of ϕ, say, $\left[0, \phi_1\right]$, $\left[\phi_1, \phi_2\right]$, $\left[\phi_2, \pi\right]$, then $f(\phi)$ can be well approximated by

$$f(\phi) = b_3\phi^2 + b_4\phi \qquad (36)$$

for each range, where b_3 and b_4 may vary somewhat between different ranges of ϕ. Equation (34) is now expressed as

$$E\phi = C_3 \int \phi\, e^{-jk(b_3\phi^2 + b_4\phi)}\, d\phi \qquad (37)$$

The square of the exponent of Eq. (37) may be completed as

$$\left(\sqrt{b_3}\,\phi + \frac{b_4}{2\sqrt{b_3}}\right)^2 - \frac{b_4^2}{2b_3} = b_3\phi^2 + b_4\phi \qquad (38)$$

Now consider the substitution $\phi' = \sqrt{b_3}\,\phi + \dfrac{b_4}{2\sqrt{b_1}}$ such that

$$\phi = \frac{\phi' - \dfrac{b_4}{2\sqrt{b_3}}}{\sqrt{b_3}} = \frac{\phi'}{\sqrt{b_3}} - \frac{b_4}{2b_3}$$

and $$d\phi = \frac{d\phi'}{\sqrt{b_3}}$$

which when made in Eq. (37) gives

$$E\phi = C_3\, e^{jk(b_4^2/2b_3)} \int e^{-jk\phi'^2} \left[\frac{\phi'}{\sqrt{b_3}} - \frac{b_4}{2b_3}\right] \frac{d\phi'}{\sqrt{b_3}}$$

$$= C_4 \int \frac{e^{-jk\phi'^2}}{b_3}\, \phi' d\phi' - C_4 \int e^{-jk\phi'^2}\, \frac{b_4}{2b_3\sqrt{b_3}}\, d\phi$$

$$= \frac{C_4}{-2jkb_3}\, e^{-jk\phi'^2} \Big|_{\phi'_1}^{\phi'^2} - \frac{C_4 b_4}{2b_3^{3/2}} \int e^{-jk\phi'^2}\, d\phi'$$

$$= \frac{C_3}{-2jkb_3}\, e^{-jk\left[b_3\phi^2 + b_4\phi\right]} \Big|_{\phi_1}^{\phi_2} - \frac{C_4 b_4}{2b_3^{3/2}} \int e^{-jk\phi'^2}\, d\phi' \qquad (39)$$

The first term of Eq. (39), when evaluated, yields some complex number. The second term is in the form of a Fresnel integral for which values have been tabulated (Schelkunoff, 1948). The integral is separated into its real and imaginary parts, and these parts are defined as

$$C(x) = \int_0^x \cos\left(\frac{\pi t^2}{2}\right) dt, \quad S(x) = \int_0^x \sin\left(\frac{\pi t^2}{2}\right) dt \qquad (40)$$

The Fresnel integral for a more general argument is given as

$$\int_0^x \sin(zt^2)\, dt = \sqrt{\frac{\pi}{2z}}\; S\left(\sqrt{\frac{2z}{\pi}}\, t\right) \qquad (41)$$

and similarly for C(x). A graph of the functions C(x) and S(x) is given in Fig. 14. It may be observed that both C(x) and S(x) start from zero, rise to a maximum value of between 0.7 and 0.8, and then their values oscillate about 0.5.

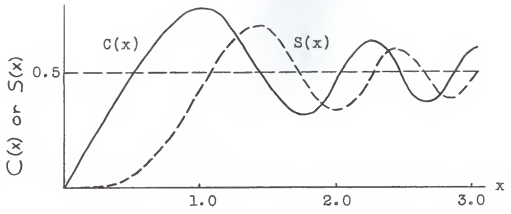

Fig. 14. The Fresnel integrals.

The orthogonal component of $\bar{E}$ can be expressed similarly as

$$E_\theta = C_3 \cos\theta \int e^{-jk\left[f(\phi)\right]}\, d\phi \tag{33}$$

$$= C_3 \frac{\cos\theta\, e^{j(kb_4{}^2/2b_3)}}{\sqrt{b_3}} \int e^{-jk\phi'^2}\, d\phi' \tag{42}$$

where b_3, b_4, and ϕ' are the same as defined previously. Equations (39) and (42) were derived for the real antenna, and corresponding expressions for the image antenna can be worked out in identical manner after making the appropriate sign changes as indicated in Eq. (12).

The quantities b_3 and b_4 can be solved by curve fitting techniques for variable θ and a fixed ϕ_0, or a variable ϕ_0 and a given θ. This permits the evaluation of E_θ and E_ϕ over the hemisphere $\left[0 \leq \theta \leq 180^\circ,\ 0 \leq \phi \leq 180^\circ\right]$. The calculation of b_3 and b_4 is long and complex but exact values of these quantities are not necessary to determine the general shape of the field patterns from Eqs. (39) and (42).

Interpretation of Field Equations

Equation (39) is difficult to interpret, being a sum of two complex numbers. Each term of Eq. (39) is a different function of ϕ, ϕ_0, and θ, so the pattern for, say, $\theta = 90°$ appears to be difficult to describe mathematically. Intuitively, E_ϕ for $\theta = 90°$ could be relatively constant for some range of ϕ_0, or could even be zero for a particular ϕ_0. This would seem to indicate that the observed pattern of E_ϕ, $\theta = 90°$ (Fig. 6), is theoretically possible to obtain from Eq. (39).

The plot of E_ϕ for $\phi_0 = 90°$ may be deduced from the fact that the ϕ' of the Fresnel integral involves a sin θ term. This variation of ϕ' with respect to θ could cause C(x) and S(x) to vary over one or more of their maximums shown in Fig. 13. If this is the case, then the lobes of Figs. 6 and 7 can be explained by Eq. (39), or vice versa.

Equation (42) shows that $E_\theta = 0$ for $\theta = 90°$, which is verified by experimental results. It also shows a predominantly cos θ variation of E_θ, which agrees with the experimental data as well. Variation of ϕ' with respect to θ in the Fresnel integral also affects E_θ for $\phi_0 = 90°$, which prevents the patterns in Figs. 6 and 7 from being strictly cos θ in shape. The patterns actually appear to have a $\cos^2 \theta$ variation rather than cos θ. A plot of Eq. (42) for the Archimedes scimitar is given in Fig. 15.

The explanations in the above paragraphs are not rigorous but it appears that Eq. (42) contains the same general variation of E_θ as observed experimentally, while Eq. (39) seems to have

the same general variation of E_ϕ, depending on several constants involved. A plot of Eq. (39) for $\theta = 90°$, Fig. 15, is similar in general shape with that obtained experimentally, especially the sharp null at about $\phi_0 = 140°$. Figure 15 has included contributions from both the real and image antennas, of course.

CONCLUSIONS

The scimitar antenna has been shown to be one of a class of broadband antennas. It is truly frequency independent since it does not have an inherent upper cut-off frequency, and the lower cut-off frequency is limited only by the length of the outer curve of the scimitar. An extension of the bandwidth is a practical matter since the outer curve need only be one wavelength at the lowest frequency of operation, and this extension to a larger antenna will not affect its high efficiency or its power handling capabilities.

The input impedance converges to 50 ohms resistance with increasing frequency, and the VSWR is below two-to-one to a 50-ohm line over at least a ten-to-one band width.

The antenna will radiate in all directions above its ground plane, with the possible exception of a null or two in the plane of the antenna.

Approximate far field equations are derived and are shown to agree with radiation patterns obtained experimentally insofar as the essential characteristics are concerned.

Further work is required to study some of the unknowns of

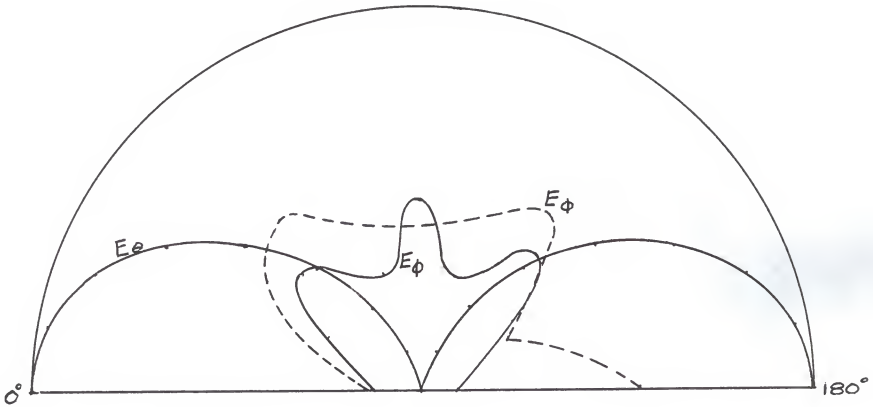

Fig. 15. Theoretical field strength patterns for Archimedes scimitar antenna, r = k0.

$\emptyset$ = 90°, θ variable.

θ = 90°, $\emptyset$ variable (E_θ = 0).

the antenna, such as direction of current flow, rate of attenuation of current along the antenna, velocity of propagation along the antenna, and the effect of width of the antenna arm on antenna operation.

The Archimedes and the equiangular scimitars have very similar experimental characteristics, so it is difficult to draw any conclusions as to the superiority of either antenna. The theoretical field equations are also similar for the two antennas, but a more extensive study of these equations should indicate which antenna best meets a particular criterion of, say, least pattern variation with respect to frequency or with respect to direction from the antenna.

The major disadvantage of the scimitar antenna is that its gain is not superior to that of a half-wave dipole. However, this antenna has a number of important advantages. It needs no special matching or coupling networks for use with a single transmitter. It is easy to construct with less critical tolerances than many other antennas in this frequency range. It has excellent mechanical strength because of its large base-to-height ratio. Antenna efficiency of above 60 per cent may be obtained. The scimitar antenna exhibits band widths between 10:1 and 20:1. These advantages make the scimitar particularly desirable for airborne antenna applications.

REFERENCES

1. Curtis, Walter L.
Spiral antennas. IRE Trans. on Antennas and Propagation, Vol. AP-8, No. 3. pp. 298-306. May, 1960.

2. Dyson, John D.
The equiangular spiral antenna. University of Illinois Engineering Experiment Station. Antenna Laboratory Technical Report No. 21. Contract No. AF33(616)-3220. Project No. 6(7-4600), task 40572. Wright Air Development Center. 15 September 1957.

3. Hayt, William H., Jr.
Engineering electromagnetics. New York: McGraw-Hill, 1958.

4. Kraus, John D.
Antennas. New York: McGraw-Hill, 1950.

5. Riblet, H. B.
A broadband spherical satellite antenna. Proc. of the IRE. pp. 48-631. 1960.

6. Rumsey, V. H.
A new way of solving Maxwell's equations. IRE Trans. on Antennas and Propagation, Vol. AP-9, No. 5. pp. 461-465. September, 1961.

7. Rumsey, V. H., B.R.S. Cheo, W. J. Welch.
A solution to the frequency-independent antenna problem. IRE Trans. on Antennas and Propagation, Vol. AP-9, No. 6. pp. 527-534. November, 1961.

8. Schelkunoff, S. A.
Applied mathematics for engineers and scientists. New York: D. Van Nostrand Company, 1948. pp. 385-388.

9. Stratton, Julius Adams.
Electromagnetic theory. New York: McGraw-Hill, 1941.

THE SCIMITAR ANTENNA

by

GARY LEE JOHNSON

B. S., Kansas State University, 1961

AN ABSTRACT OF
A MASTER'S THESIS

submitted in partial fulfillment of the

requirements for the degree

MASTER OF SCIENCE

Department of Electrical Engineering

KANSAS STATE UNIVERSITY
Manhattan, Kansas

1963

The scimitar antenna is a broadband antenna of the same class as the spiral antenna, and is similar to a spiral antenna of one-half revolution terminated on a transverse ground plane. The performance of two types of scimitar antennas, equiangular and Archimedes, is determined experimentally. The theoretical far field is calculated for a narrow Archimedes scimitar using an assumed current distribution and image theory. This far field is shown to agree in essential characteristics with the far field obtained experimentally. Experimental results also show that either scimitar type possesses a voltage standing wave ratio of below 2:1 over a frequency range of 10:1. The input impedance is nearly 50 ohms resistive without matching networks. Radiation patterns are similar to those of the spiral antenna, except that the scimitar also radiates in the plane of the antenna.